Atmospheric Environment 220 (2020) 117060

Contents lists available at ScienceDirect

Atmospheric Environment

journal homepage: http://www.elsevier.com/locate/atmosenv

The role of natural factors in constraining long-term tropospheric ozone trends over Southern China

Xi Chen [a,b], Buqing Zhong [c], Fuxiang Huang [b,*], Xuemei Wang [c], Sayantan Sarkar [d], Shiguo Jia [g,h], Xuejiao Deng [e], Duohong Chen [f], Min Shao [c]

[a] School of Environmental Science and Engineering, Sun Yat-sen University, Guangzhou 510275, PR China
[b] National Satellite Meteorological Center, Beijing 100081, PR China
[c] Institute for Environmental and Climate Research, Jinan University, Guangzhou 511486, PR China
[d] Department of Earth Sciences, Centre for Climate and Environmental Studies, Indian Institute of Science Education and Research (IISER) – Kolkata, Nadia, 741246, West Bengal, India
[e] The Institute of Tropical and Marine Meteorology, CMA, Guangzhou 510640, PR China
[f] Guangdong Environmental Monitoring Center, State Environmental Protection Key Laboratory of Regional Air Quality Monitoring, Guangzhou 510308, PR China
[g] School of Atmospheric Sciences, & Guangdong Province Key Laboratory for Climate Change and Natural Disaster Studies, Sun Yat-sen University, Guangzhou 510275, PR China
[h] Southern Laboratory of Ocean Science and Engineering (Guangdong, Zhuhai), Zhuhai 519000, PR China

HIGHLIGHTS

- The increasing rates of tropospheric column ozone and surface ozone are 0.28 DU y^{-1} and 0.23 ppbv y^{-1}, respectively.
- Natural factors explain 44% and 27% of the tropospheric column ozone and surface ozone upward trends, respectively.
- Solar irradiance cycle is the main natural cause of long-term ozone increase.
- The Asian summer monsoon has a strong scavenging effect on summertime ozone.
- More than half of the upward trends remain unexplained which are most likely related to anthropogenic emissions.

ARTICLE INFO

Keywords:
Tropospheric ozone
Solar cycle
Wet deposition
Surface wind
Asian summer monsoon

ABSTRACT

Southern China has experienced severe photochemical pollution events in recent years, and the tropospheric ozone has emerged as the major pollutant of concern. Despite some recent efforts, the role of natural factors in constraining long-term trends of ozone in this region is poorly understood. In this study, we addressed this issue using tropospheric column ozone (TCO) datasets (2005–2017) from the Ozone Monitoring Instrument/Microwave Limb Sounder (OMI/MLS) and surface ozone datasets from 16 monitoring stations in Southern China (2006–2016). Consequently, we studied the influence of atmospheric dynamical factors, such as solar cycle, El-Nino Southern Oscillation (ENSO), Quasi-Biennial Oscillation (QBO), and Arctic Oscillation (AO), and local-scale meteorological factors, such as precipitation, surface temperature, planetary boundary layer height, and horizontal winds, on regional ozone trends. Stepwise multivariate regression analysis and harmonic function fitting were adopted to quantitatively simulate the influence of these natural drivers on ozone change. We found that within our research periods, both surface ozone and TCO in Southern China had a significant upward trend, with slopes of 0.97% y^{-1} (0.23 ppbv y^{-1}) and 0.82% y^{-1} (0.28 DU y^{-1}), respectively. Natural factors explained 44.4% of the TCO uptrend and 27.0% of the surface ozone uptrend. Among the natural factors, the solar cycle plays the most important role in tropospheric and surface ozone modulation. Its 11-year cycle had a large impact on TCO for 2–7 DU and on surface ozone for 3–8 ppbv. However, the ENSO, QBO, and AO indices did not affect tropospheric ozone trends significantly. In addition, we showed that precipitation and wind fields associated with the Asian summer monsoon played a critical role in lowering ozone levels over Southern China, accounting for 24.8% and 81.5% of summertime TCO and surface ozone variability, respectively. Finally, a significant fraction of TCO and surface ozone uptrends (55.6% and 73.0%, respectively) remained unexplained even after

* Corresponding author.
E-mail address: huangfx@cma.cn (F. Huang).

https://doi.org/10.1016/j.atmosenv.2019.117060
Received 14 May 2019; Received in revised form 9 October 2019; Accepted 15 October 2019
Available online 21 October 2019

consideration of these natural factors in the periods 2005–2017 and 2006–2016, respectively. These unexplained factors are most likely related to anthropogenic emissions and should be studied further.

1. Introduction

Tropospheric ozone is an important greenhouse gas, with an estimated direct radiative forcing (RF) of 0.40 (0.20–0.60) W m^{-2} during the industrial era (IPCC, 2013). Its production depends on photochemical reactions of its precursors as well as stratosphere-troposphere exchange (Logan, 1985; Holton et al., 1995; Uno et al., 1998; Greenslade et al., 2017). Tropospheric ozone is not only affected by anthropogenic and biogenic emissions of precursors (Tang et al., 2009; Xu et al., 2018; Lal et al., 2012); it is also influenced considerably by natural factors, such as circulation and meteorology (Doherty et al., 2006; Nassar et al., 2009; Lin et al., 2014., Edwards et al., 2018). Ozone changes in the upper troposphere are expected to have a considerable impact on global warming, along with effects on moisture levels, cloud amount and distribution, precipitation, and atmospheric dynamics on various scales (Mohnen et al., 1993). The RF from ozone is strongly latitude-dependent, and consequently, it is necessary to accurately estimate changes in ozone's spatial-temporal structure using models and observations (IPCC, 2013). At the surface, ozone is an air pollutant that adversely impacts human health, natural vegetation, and crop yield and quality (Cooper et al., 2014). For these reasons, the factors that constrain tropospheric ozone and surface ozone levels and influence its long-term trends have received widespread attention in recent years.

The analysis of tropospheric ozone trends mainly depends on ground-based observations, ozone sounding from aircraft observations, and satellite remote sensors (Oltmans et al., 2006, 2013; Nassar et al., 2009; Lin et al., 2014). Satellite remote sensing has the prominent advantage of better spatial coverage and temporal continuity when compared to ground stations. Since the 1990s, the NASA Langley Research Center has maintained a remote sensing dataset of tropospheric, total, and vertical profiles of ozone (Fishman et al., 1990, 2003; 2005; Chandra et al., 2003; Ziemke et al., 1998, 2006; 2011, 2019; Kulkarni et al., 2010). This dataset is built by the tropospheric residual (TOR) method, whereby satellite observations and total ozone soundings from, for example, the Aura Ozone Monitoring Instrument (OMI) and Aura Microwave Limb Sounder (MLS), are used to determine the tropopause height, followed by generation of tropospheric ozone products. The generated tropospheric ozone data were initially limited to $\pm 50^{\circ}$ from the equator (Fishman et al., 1990, 2003; 2005; Chandra et al., 2003), but it was later extended to $\pm 60^{\circ}$ (Ziemke et al., 1998, 2006; 2011; Kulkarni et al., 2010). Although the OMI/MLS tropospheric column ozone (TCO) retrievals effectively indicate tropospheric ozone accumulation, they are not sensitive to surface ozone mixing ratios (Ziemke et al., 2011), and analysis of surface ozone still depends on surface observations. Therefore, TCO analysis and surface ozone measurements must be conducted in tandem for a comprehensive understanding of tropospheric ozone trends, the influence of local meteorology, and synoptic scale atmospheric processes on ozone.

Within our research periods, a large number of studies have investigated the long-term trends of tropospheric ozone on regional and global scales (Ziemke et al., 1999, 2000; 2019; Cooper et al., 2014; Oltmans et al., 2006, 2013; Nassar et al., 2009). For China, previous studies have shown that there is a significant upward trend in TCO (Beig and Singh, 2007; Shen and Wang, 2012) and surface ozone (Tang et al., 2009; Chen et al., 2018). However, for a country as large as China, significant spatial heterogeneities exist pertaining to the emission of ozone precursors, meteorological parameters, and synoptic scale atmospheric conditions, which can influence tropospheric ozone trends on regional scales. Targeted studies on TCO and surface ozone in regions of China that are most susceptible to photochemical pollution are therefore strongly warranted. In this regard, a special region of interest is Southern China, which, as an important industrial and economic center for the country, has in recent times experienced severe photochemical pollution events characterized by high levels of ozone and haze phenomena dominated by high concentrations of fine particles ($PM_{2.5}$) (Wang and Hao, 2012; Zhong et al., 2013). With the effectiveness of the local government's control of $PM_{2.5}$, ozone has currently become the most important pollutant in Southern China (Guangdong Provincial Environmental Monitoring and Environmental Protection, 2006, 2014). Concerted efforts are required to understand the influence of natural and anthropogenic factors on levels and long-term trends of tropospheric ozone in this region.

As mentioned previously, trends of tropospheric ozone are not only closely related to photochemical production, which varies with location, but are also correlated to thermal, dynamical, and other natural factors that have spatial variations of their own (Doherty et al., 2006; Nassar et al., 2009; Lin et al., 2014). For example, Ziemke et al. (1999) showed that TCO in the Eastern Pacific, Atlantic, and Western Pacific was influenced by the El Nino Southern Oscillation (ENSO), the Quasi-Biennial Oscillation (QBO), and the solar cycle. Huang et al. (2009) indicated that there exists a solar cycle-dependent trend in tropospheric ozone over the Tibetan Plateau. The Asian summer monsoon (ASM) has been shown to be a major atmospheric system influencing the distribution of ozone and its precursors in the Asian monsoon region during the summer (Li et al., 2018; Worden et al., 2009; Zhao et al., 2010), affecting air mass transport, convection, and precipitation (Zhao et al., 2010). The convection associated with the ASM transports air masses with low ozone and high water vapor from the marine boundary layer into the upper troposphere, thereby affecting both ground-level and column-integrated tropospheric ozone (Randel et al., 2010). In China, previous research on this issue has mainly focused on the impact of anthropogenic emissions (Tang et al., 2009; Lee et al., 2014) and associated heavy pollution episodes (Che et al., 2011; Jiang et al., 2008), and there exists an acute lack of research on the role of natural factors in constraining the long-term trend of ozone. In the present study, we address precisely this issue by combining ground- and satellite-based measurements to analyze the trends of ozone and to quantitatively assess the influence of major natural factors over Southern China. We believe the results of this study will act as a much-needed reference point for understanding regional air quality in this area.

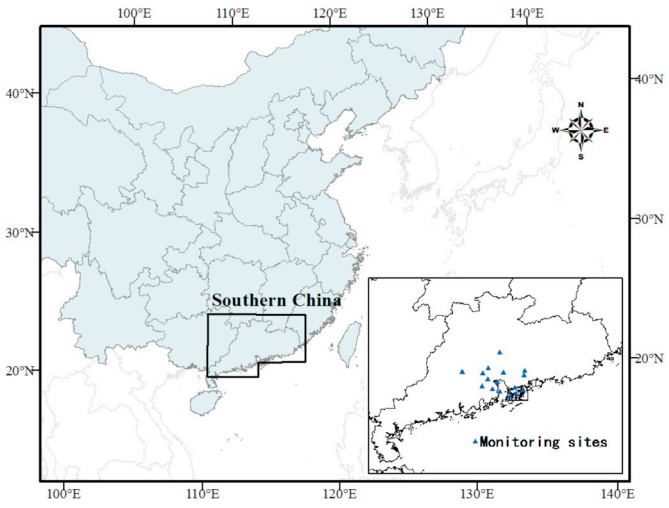

Fig. 1. Map of Southern China (study area), and locations of surface observation sites.

2. Materials and methods

2.1. Study area

The study area for the present work was Southern China (20°-25.5°N, 109.5°-117°E; Fig. 1), which has borders with Hong Kong, Macao, Guangxi, Hunan, Jiangxi, and Fujian. The focus is on Guangdong Province, which consists of four regions: Eastern, Western, and Northern Guangdong and the Pearl River Delta. This region has been the dominant driver of the national economy for the past 3 decades, and since 1989, Guangdong's GDP has consistently occupied first place within 30 provinces and cities in China (data from National Bureau of Statistics). To better understand the role of natural factors specific to Southern China in constraining tropospheric ozone, we used measurements over Northern China (35°-42°N, 110°-120°E; Fig. S1, Supporting Information) as a control group. The control area in question is the Beijing-Tianjin-Hebei region, which is the political, economic, and cultural center of Northern China. The problem of atmospheric ozone pollution in this area is also significant, but it is less affected by the ASM by virtue of its location to the north (Wu et al., 2013).

2.2. Data sources

In this study, we used two ozone datasets: a TCO dataset and a surface ozone observation dataset. The TCO dataset was constructed from monthly means of tropospheric ozone from January 2005 to December 2017. It was generated by Ziemke et al. (2006) using OMI and MLS remote sensing products with a spatial resolution of $1^\circ \times 1.25^\circ$. The monthly mean surface ozone measurements were provided by the Guangdong-Hong Kong-Macao Pearl River Delta Regional Air Quality Monitoring Network (https://www.gdep.gov.cn/hjjce/kqjc/) and the Beijing Municipal Environmental Monitoring Center (http://www.bjmemc.com.cn/). There are 16 observation sites in Southern China, marked with blue triangles in Fig. 1 and 34 observation sites in Northern China, marked with blue circles in Fig. S1.

To study the effects of regional climatic parameters on ozone levels in Southern China, the following variables were considered: i) solar radiation cycle data (www.ngdc.noaa.gov): this refers to the monthly mean of solar irradiance at F10.7 cm after Earth-Sun distance correction given in Solar Flux Units (SFU), where $1\ \mathrm{SFU} = 10^{-22}\ \mathrm{W\,m^{-2}\ Hz^{-1}}$ (Deland and Cebula, 2008; Huang et al., 2013); ii) ozone ENSO index (http://acdb-ext.gsfc.nasa.gov/Data_services/cloud_slice/index.html): a large number of ENSO type indices exist; here, the monthly ozone ENSO index from 2005 to 2015 was used. This index specifically examines the impacts of ENSO on tropospheric ozone changes using temperature outliers (Ziemke et al., 2010; Oman et al., 2011); iii) QBO index(https://acdb-ext.gsfc.nasa.gov/Data_services/met/qbo/QBO_Singapore_Uvals_GSFC.txt): this refers to the calculated empirical orthogonal functions (EOF) data sequence of the wind velocity (in m s^{-1}) at 70 hPa in Singapore (1°N, 140°E) (Ziemke and Chandra, 1999); and iv) Arctic Oscillation (AO) index: the daily AO index is constructed by projecting the 1000 hPa height anomalies poleward of 20°N onto the loading pattern of the AO and is obtained from the NOAA National Weather Service Climate Prediction Center website (http://www.cpc.ncep.noaa.gov/products/precip/CWlink/daily_ao_index/teleconnections.shtml). Additionally, the monthly mean tropopause pressure was derived from the National Centers for Environmental Prediction (NCEP) reanalysis data(https://www.ncep.noaa.gov/) with a spatial resolution of $2.5^\circ \times 2.5^\circ$. Precipitation, surface temperature, planetary boundary layer height (PBLH), and horizontal wind (300 hPa, 600 hPa, and 1000 hPa) were taken from the ERA-Interim dataset of the European Centre for Medium-Range Weather Forecasts (ECMWF)(https://www.ecmwf.int/en/forecasts/datasets/reanalysis-datasets/era-interim). The spatial resolution of the ERA-Interim dataset was $0.25^\circ \times 0.25^\circ$.

2.3. Statistical analyses

The Mann-Kendall (MK) test was used for trend analysis. It is a non-parametric rank correlation test that uses the relationship between continuous data to check whether the trend is significant. Advantages of this method include no strict assumptions on the distribution of the data sequence (such as the normal distribution hypothesis) and the ability to handle extreme values as well as missing data. This method is suitable for analyzing trends in atmospheric and hydrological data (Gocic and Trajkovic, 2013; Zhou et al., 2017). The trend slope was calculated by the Theil-Sen slope estimation method. When time series data exhibits a characteristic linear trend, its slope can be determined using the following simple equation:

$$\beta = \mathrm{median}\left(\frac{x_j - x_k}{j-k}\right) j = 1, 2, \ldots, n; \quad k = 1, 2, \ldots, j-1 \tag{1}$$

In Eq. (1), β is the slope between two data points in the time series, while $x_j$and x_k are the data values corresponding to j-th and k-th time points ($j > k$). The advantage of this parameter is that it provides an accurate confidence interval for the trend of the time series data itself even in the case of non-normally distributed data and in the presence of heteroscedasticity (Gocic and Trajkovic, 2013). The linear fit was used to analyze the influence of each item (different factors) in the multiple linear regression (MLR) equation on the interannual trend of ozone and to compare it with the results of the MK test. For details, please see Section 3.2. MLR analysis was used here to study the effects of climatic variables on ozone levels. MLR is one of the most widely used methodologies for expressing the dependence of a response variable on several independent (predictor) variables (Abdul-Wahab et al., 2005; Steinbrecht et al., 2011; Chehade et al., 2014). In spite of its evident success in many applications, the regression approach can face serious difficulties when independent variables are correlated with each other (McAdams et al., 2000; Abdul-Wahab et al., 2005). To eliminate the impact of potential correlations between variables on regression results, forward stepwise regression analysis was used to screen the variables (Chen et al., 2014). Stepwise regression analysis first uses the explanatory variables to make a simple regression for each of the explanatory variables considered. Based on the regression equation corresponding to the variable with the largest contribution, the remaining explanatory variables are gradually introduced, F-test and t-test are performed on each added variable, and insignificant variables are eliminated. After a stepwise regression, the explanatory variables that are finally retained in the model are both important and have no serious multicollinearity. In the study area, there were 34 satellite grid points and 16 observation sites. Therefore, the screening test was divided into two groups. Stepwise regression analysis was performed for each of the satellite data and ground observation data to examine the significance of different factors in each set of data.

After variable selection, a multivariate linear regression equation was built using significant variables to fit the regional average ozone (Ziemke and Chandra, 1999):

$$TCO(t)\,/\,GLO(t) = \alpha + \beta t + \gamma VAR1(t) + \delta VAR2(t) + \varepsilon VAR3(t) + \varepsilon VAR4(t) + \ldots + R(t) \tag{2}$$

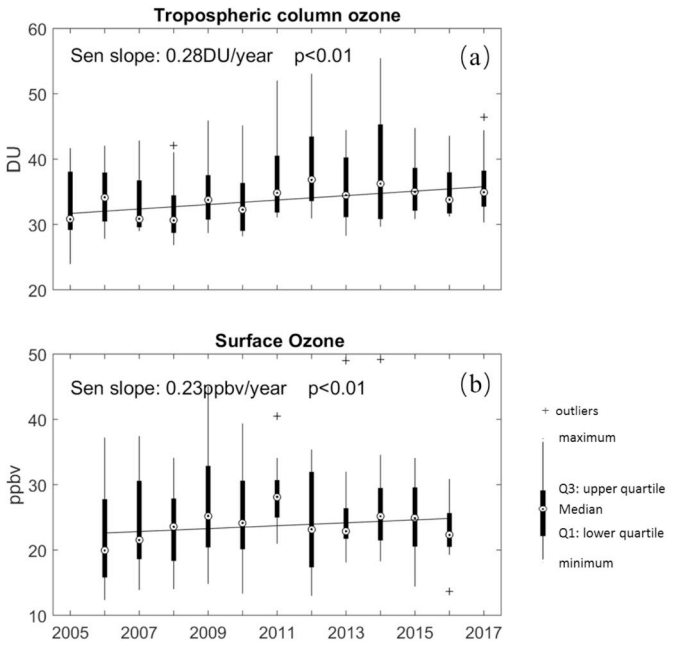

Fig. 2. Interannual trends of TCO and surface ozone over Southern China. Sen slope from MK test (see Eq. (1) for details).

In Eq. (2), TCO(t) and GLO(t) denote tropospheric column and surface ozone, respectively. α represents a constant term, t represents the month number ($t = 1, 2, ..., 156$ corresponding to January 2005 through December 2017), $\beta,\gamma,\delta,\varepsilon$, and ε are the regression coefficients of the time-varying covariates, and R is the residual error term between the observation data and numerical simulation. For variables with cyclical changes, the regression coefficients ($\beta,\gamma,\delta,\varepsilon$, ε) are follow harmonic functions with cycles of 12 and 6 months in order to improve simulation results. The function is expressed in the following form:

$$\beta = c_0 + \sum_{j=1}^{2}\left[c_j \cos(2\pi jt/12) + s_j \sin(2\pi jt/12)\right]. \quad (3)$$

3. Results and discussion

3.1. Ozone trends over Southern China within our research periods

The MK test was used to analyze the interannual (monthly mean) and seasonal (seasonal mean) trends of tropospheric ozone from 2005 to 2017 and surface ozone from 2006 to 2016. From the perspective of interannual variation, both TCO and surface ozone show significant ($p < 0.01$) increasing trends (Fig. 2). The rate of increase of surface ozone is slightly higher than that of TCO, with slopes of 0.97% y^{-1} (0.23 ppbv y^{-1}) and 0.82% y^{-1} (0.28 DU y^{-1}), respectively. Previous studies have also reported a rising trend in surface ozone in Southern China, which has been shown to be associated with changes of ozone precursors (Lee et al., 2014; Wang et al., 2009, Li et al., 2018); however, the role of natural factors in constraining surface and tropospheric ozone trends remains inconsistent (Lou et al., 2015; Sun et al., 2019; Xu et al., 2018). We note that this rising trend of surface ozone in Southern China is in agreement with the first Tropospheric Ozone Assessment Report (TOAR) (https://collections.elementascience.org/toar?rq=TOAR), which indicated significant negative trends in surface ozone at most US and some European sites and significant positive trends at many sites in East Asia between 2000 and 2014 (Fleming et al., 2018; Mills et al., 2018; Young et al., 2018; Chang et al., 2017).

Table 1
Seasonal and annual slopes from MK test and corresponding p values of tropospheric ozone and surface ozone. The numbers in parentheses indicate the upper 95% and lower 95% slopes.

	Annual	MAM	JJA	SON	DJF
Tropospheric column ozone(DU yr-1)	0.28 (0.24, 0.33) $p < 0.05$	0.51 (0.15, 0.96) $p < 0.05$	0.24 (-0.04, 0.51) $p = 0.1$	0.32 (0.08, 0.50) $p < 0.05$	0.29 (0.04, 0.59) $p < 0.05$
Surface ozone(ppbv yr-1)	0.23 (0.10, 0.34) $p < 0.05$	−0.11 (-1.29, 1.05) $p = 0.82$	1.19 (0.25, 2.06) $p < 0.05$	−0.74 (-2.09, 0.40) $p = 0.31$	−0.53 (-1.69, 0.78) $p = 0.43$

To further investigate the trend of ozone in different seasons, the trend of seasonal average ozone was calculated and is shown in Figs. S2 and S3, and the slope and p values from the MK test are listed in Table 1. The strongest increase in TCO was found in spring (MAM), followed by autumn (SON) and then winter (DJF), reaching 0.51, 0.32 and 0.28 DU $year^{-1}$, respectively. In comparison, summer (JJA) shows much weaker increasing trends, with rates of 0.24 $year^{-1}$, and the summertime trend does not reach a confidence level of 95%. However, surface ozone showed a significant upward trend only in summer (1.19 ppbv $year^{-1}$), while other seasons showed a downward trend; however, neither trends reached a confidence level of 95%.

The differences in the annual cycles of ozone between 2006-2011 and 2011–2016 are shown in Fig. 3. Compared with the previous period (2006–2011), in recent years (2011–2016), TCO increased across all 12 months, with enhancements ranging from 0.9 DU in July to 4.9 DU in April. In comparison, the surface ozone decreased in February, May, November, and December, with a range of reduction from −0.35 ppbv in February to −5.1 ppbv in April, and increased in the remaining months, with a range from 0.3 ppbv in September to 3.9 ppbv in June. We discuss potential effects of natural factors on the observed surface and tropospheric ozone trends in the next section.

3.2. Natural factors affecting TCO and surface ozone

This section aims to analyze the influence of natural factors on TCO and surface ozone over Southern China. First, stepwise regression analysis was used to filter variables. Solar radiation cycle, QBO, ENSO, and AO index, which characterize large-scale circulation and climatic conditions, are thought to have a significant impact on total column ozone, but their effects on tropospheric ozone are not known explicitly (Chehade et al., 2014). In addition, for surface ozone, the impact of local meteorological factors cannot be ignored. Therefore, in addition to the four factors mentioned above, tropopause pressure, surface temperature, precipitation, PBLH, and V-direction wind fields at 300 hPa, 600 hPa, and 1000 hPa were extracted.

Results of the variable screening and the influence of individual factors on TCO and surface ozone levels in Southern China are depicted in Fig. 4. First, we discuss the effects of large-scale atmospheric processes on TCO and surface ozone, followed by that of local meteorological factors. For ozone grid data from satellites ($1^\circ \times 1.25^\circ$) and ozone data from ground observations, we performed stepwise regression analysis for each grid point and each observation site to determine the significance probabilities of different factors. The significance probability is defined as the ratio of the number of significant points of the factor to the total number of grid points (for example, in Fig. 4a, ENSO is significant at 14 grid points, and the total number of grid points is 34, so the significance probability is 14/34*100% = 35.3%). The equatorial Pacific ENSO characterizes planetary-scale interannual fluctuations of the sea surface temperature, ocean currents, surface air pressure, air temperature, wind, cloud, precipitation, and tropospheric trace gases (Chandra et al., 2003). However, this factor is not significant in most of Southern China, with significance probabilities of 35.3% and 37.5% for TCO and surface ozone, respectively. The changes in the intensity of

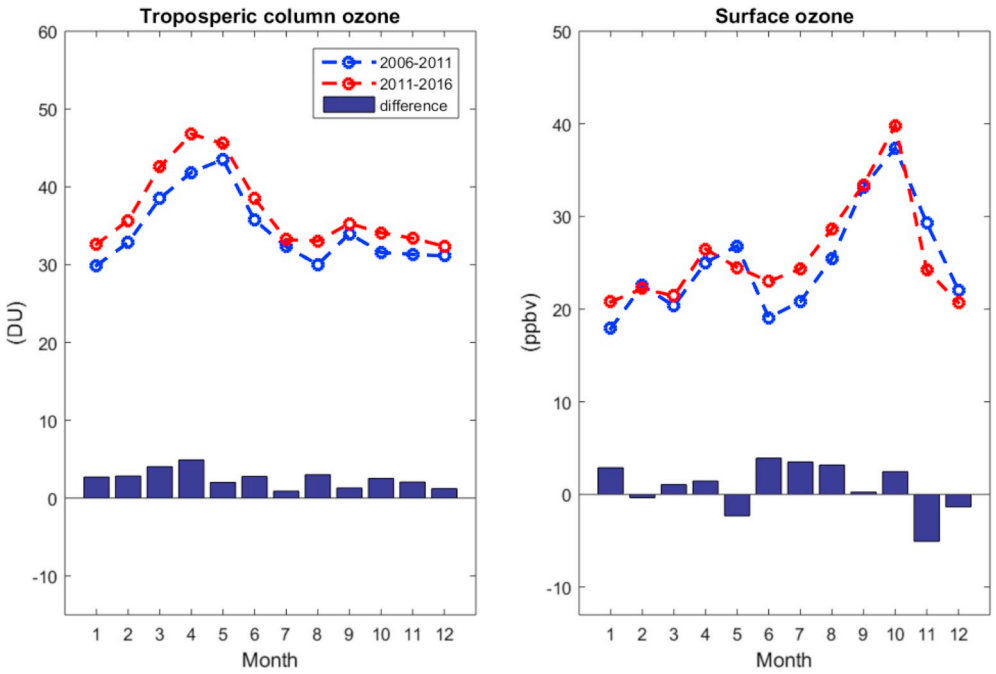

Fig. 3. Differences in the annual cycles of ozone between 2006-2011 and 2011–2016 over Southern China.

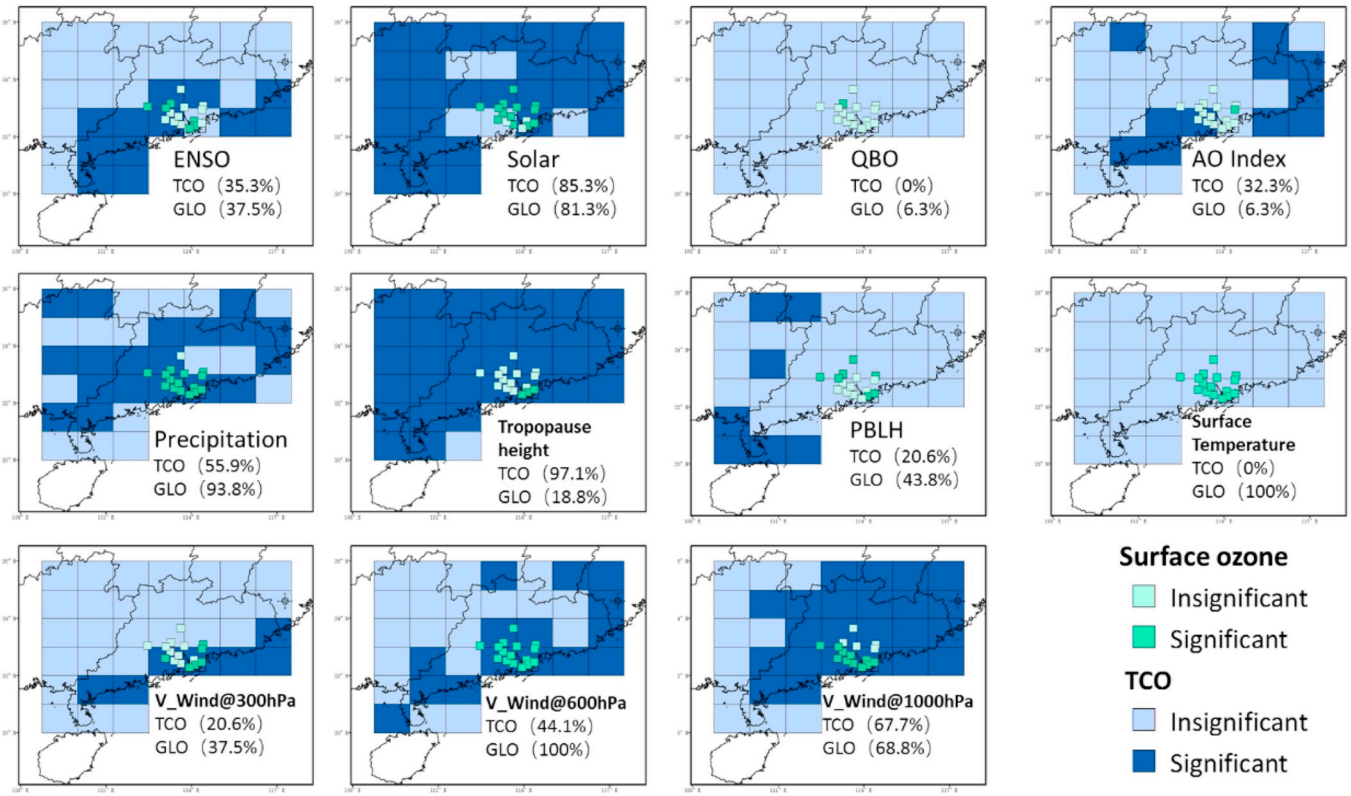

Fig. 4. Significance of large-scale climatic and local meteorological factors in constraining TCO and surface ozone over Southern China.

solar ultraviolet radiation impact both stratospheric and tropospheric ozone through photolysis, leading to the production/removal of ozone (Ziemke and Chandra, 1999; Randel and Cobb, 1994; Chandra et al., 1999). Because the solar cycle is closely related to the radiation budget of the atmosphere, both TCO and surface ozone are affected by this factor with significance probabilities of 85.3% and 81.3%, respectively. The equatorial stratosphere is characterized by the slow recurring QBO, which influences the interannual variability of total ozone columns (Baldwin et al., 2001; Chehade et al., 2014). From statistical results, it is apparent that the QBO does not play a significant role in constraining tropospheric ozone in Southern China. The AO index represents an important mode of atmospheric circulation in the mid-high latitudes of the Northern hemisphere in the winter half year that influences mid-latitude total ozone (Fusco and Salby, 1999; Steinbrecht et al.,

2011). However, based on our analysis, the significance probability of the AO index in affecting TCO in Southern China is only 32.3%, while that for surface ozone is only 6.3%. Although previous studies have shown that large-scale circulation parameters, such as ENSO, QBO, and AO index, have considerable effects on total ozone within 60°S and 60°N (Ziemke et al., 2005; Chehade et al., 2014) and tropospheric ozone in India (Lal et al., 2012), it appears from our analysis that these do not affect TCO and surface ozone levels significantly over Southern China.

Among local meteorological factors, precipitation has a significant effect on surface ozone (93.8%), which is also reflected throughout the troposphere (55.9% for TCO; Muralidharan et al., 1989). The tropopause height, which determines the thickness of the troposphere, is by default an important factor affecting TCO and has a significance probability of 97.1% for TCO and 18.8% for surface ozone, as expected. The relationship between changes in the PBLH and surface ozone concentrations is very complex and is affected by meteorological conditions, convective turbulence, and ozone precursor emissions (Haman et al., 2014). Therefore, its overall probability of affecting surface ozone is low (43.8%). In contrast, surface temperature, which is a key factor in determining monthly variations of surface ozone, shows a significance probability as high as 100%. Lastly, it is clear from Fig. 4 that surface ozone is more sensitive to wind direction than TCO and that middle- and low-level winds (600 hPa and 1000 hPa) have a greater influence on ozone levels in Southern China than high-level winds (300 hPa).

Following from the discussion above, the factors with the largest significant probabilities in influencing TCO and surface ozone were selected as variables in the MLR model to simulate the regional average ozone over Southern China. The factors chosen for TCO were solar cycle, precipitation, tropopause height, V_Wind@600 hPa, and V_Wind@1000 hPa, while those for surface ozone were solar cycle, precipitation, surface temperature, V_Wind@600 hPa, and V_Wind@1000 hPa.

Fig. 5 shows the fitting results. The coefficient of determination ($R^2 = \frac{\sum_{i=1}^{N}(Sim_i-\overline{Sim})(Obs_i-\overline{Obs})}{\sqrt{\sum_{i=1}^{N}(Sim_i-\overline{Sim})^2\sum_{i=1}^{N}(Obs_i-\overline{Obs})^2}}$) and the root mean square error ($\mathrm{RMSE} = \sqrt{\frac{1}{N}\sum_{I=1}^{N}(Sim_i - Obs_i)^2}$) were used to evaluate model performance. The R^2 for TCO is 0.69 and its RMSE is 3.23 DU, while those for surface ozone are 0.76 and 3.52 ppbv, respectively. All factors included in the models passed the *t*-test ($p < 0.01$). It is therefore clear that the MLR models fitted the monthly ozone changes well, except for underestimating peak TCO and surface ozone values during certain years.

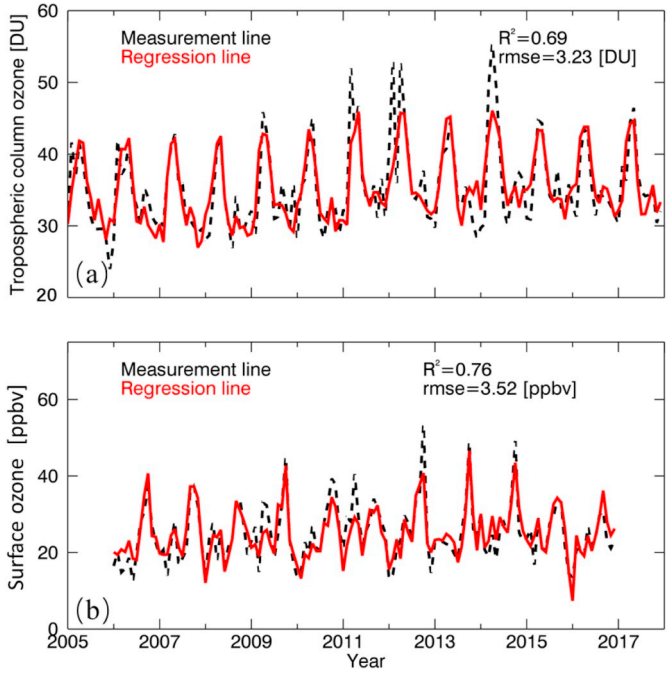

Fig. 5. Monthly mean time series of measured and modeled ozone over Southern China: (a) TCO and (b) Surface ozone.

Next, based on the MLR model, the relative contributions of explanatory factors of ozone change were determined and are shown in Fig. 6 and Fig. 7. At the same time, a linear fit was made for the contribution of different factors, and the fitted line is represented as a red line in the graph; the slope and significance statistics are listed in Table 2. "Removing all signals" in Figs. 6a and 7a indicates that the simulated ozone removes all signals in b-f, namely the *t* term plus the *R* term (residual term) in Eq. (2). Its trend indicates that which cannot be explained by the natural factors, and it has a highly significant influence on the rising trend of ozone. In Section 3.4, we discuss whether the contribution of anthropogenic sources to ozone trends is hidden within this parameter.

This section focuses on the impact of natural factors on ozone changes. The impact of natural factors on ozone is manifested in two aspects: annual cycle variation and interannual trends, which are closely related to the cyclical nature of the factors themselves. The solar cycle has a period of approximately 11 years, and it is the dominant natural factor in the long-term trend of tropospheric column ozone and surface ozone. The study period ranges from the end of the 23rd solar cycle to the end of the 24th cycle (Fig. S4a); solar activity intensified from 2006 to 2014 and has weakened since 2014. Changes in the solar cycle can affect ozone in the troposphere and surface (Figs. 6b and 7b). The contribution of the solar cycle to TCO is estimated to be between 2 DU and 7 DU, and that to surface ozone is between 3 ppbv and 8 ppbv. More importantly, the solar cycle signal showed a significant upward trend, indicating that solar radiation caused the tropospheric ozone and surface ozone to rise at rates of 0.1 DU y^{-1} and 0.24 ppbv y^{-1}, respectively. As shown in Fig. S4d, precipitation in Southern China has a distinct seasonal cycle, with the largest amount in summer and lowest in winter (Zhao et al., 2018). In summer, wet removal by precipitation reduces ozone levels, and this effect is especially noticeable in the surface ozone dataset (Fig. 7c). The precipitation signal showed a significant downward trend, indicating that the surface ozone showed a decline rate of 0.19 ppbv y^{-1}. Overall, changes in precipitation corresponded to variations of −6 to 10 DU for TCO and −3 to 13 ppbv for surface ozone.

The east wind prevails at 600 hPa over Southern China, and the absence of any obvious seasonal cycle (Fig. S4e) is consistent with the nature of atmospheric circulation in low latitudes of the northern hemisphere. The east wind brings ozone-depleted marine air masses inland, which plays a role in dilution (Figs. 6e and 7e). The V-wind at 600 hPa was responsible for TCO variations between −3 DU and 1 DU and surface ozone variations between −9 and 3 ppbv. The direction of the near-surface (1000 hPa) seasonal wind in Southern China had clear effects on TCO and surface ozone (Fig. S4f). As mentioned previously, the east wind prevails in summer, leading to a dilution of ozone over land. However, the west wind in winter transfers ozone from upwind areas to Southern China, therefore leading to a seasonal rise. The overall effect of the 1000 hPa V-wind amounts to TCO variations from −4 DU to 6 DU and surface ozone variations from −10 ppbv to 15 ppbv, due to oscillation of the east and west winds. Linear regression shows that there is no significant trend in the wind direction signal, indicating that the impact of wind direction on ozone is mainly reflected in changes in the annual cycle. The tropopause height and surface temperature are the most important factors controlling the annual cycle of tropospheric ozone and surface ozone and affect ozone variation from 20 to 40 DU and 0–35 ppbv, respectively, but their signals do not have a significant linear trend.

We compared the results of the MK trend test with the linear trend

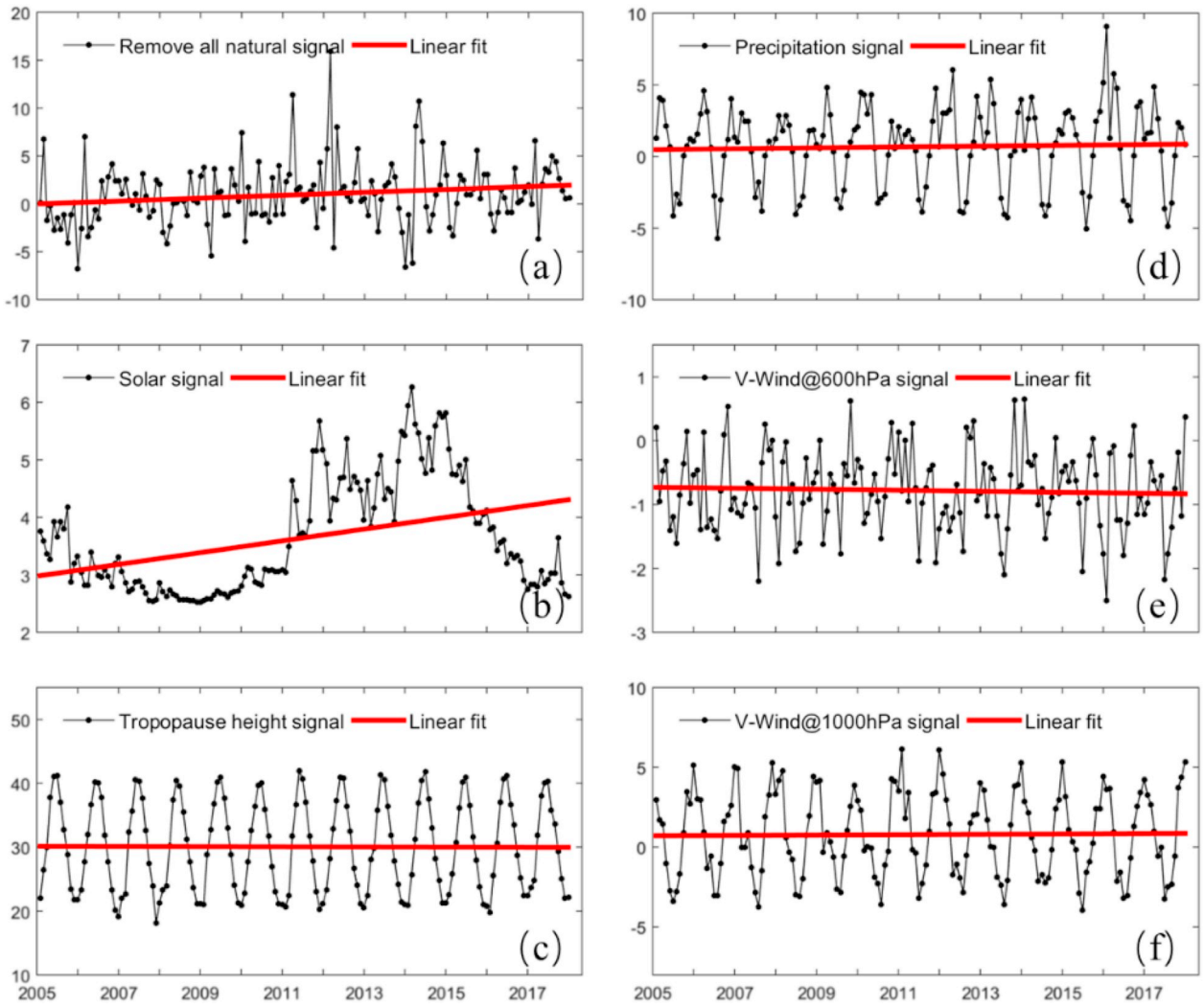

Fig. 6. Relative contributions of different signals to TCO variations over Southern China: (a) removed all natural signals, (b)solar cycle signal, (c) tropopause height signal, (d) precipitation signal, (e) V-wind@600 hPa signal, and (f) V-wind@1000 hPa signal.

analysis based on MLR. From the overall trend (total trend from MK test and MLR), the linear fit slopes and Theil–Sen trend estimates yielded very similar results.

3.3. Impact of Asian summer monsoon-related factors on ozone levels over Southern China

In Section 2.1, we noted that economic development in Southern and Northern China has been rapid, and there is a serious problem of ozone pollution. However, due to the difference in latitude, the two regions are affected by different degrees of monsoon. We compared intra-annual variations of ozone in Southern China (lower latitudes in the northern hemisphere) and Northern China (middle latitudes in the northern hemisphere) and found a large difference between the two areas, especially in summer (Fig. 8). The highest TCO was observed during June–August in Northern China, while in Southern China, the peak ozone appeared in spring, followed by a significant decline during summer. The summertime TCO difference between the two areas was 13.1 DU. A similar observation was made for surface ozone. The peak of surface ozone in Northern China appears in June, while in Southern China, the peak is in October, with a summertime difference of 22.9 ppbv. In monsoon regions, the local weather and climate, especially precipitation and wind field, are strongly influenced by monsoon circulation (Wang et al., 2008; Zhang et al., 2018). Therefore, we used precipitation and wind direction at 600 hPa and 1000 hPa as related parameters for the ASM to explore its impact on lower ozone levels in summertime over Southern China.

Fig. 9 shows the intra-annual cycle of ozone after removal/addition of the ASM-related signal (Precipitation, v_wind@600 hPa, and v_wind@1000 hPa). In Fig. 9, the black boxes represent observational values, blue boxes show results from the MLR model, and red boxes represent ozone variation after removing the ASM-related signal from the model. It is evident that the regression model captures the seasonality in ozone and simulates its intra-annual cycle very well. A large deviation from the observed profile was found when the ASM-related signal was removed from the model (blue vs red boxes). After its removal, TCO rises from January to May and falls thereafter, while surface ozone rises from January to August, followed by a decline. Among seasons, the largest deviations from observational data are seen for summer. If the influence of the ASM-related signal is removed, TCO will increase by 8.2 DU from June to August, accounting for 24.8% of summertime ozone, thereby reducing the summertime TCO difference from Northern China from 13.1 DU to 4.9 DU. On the other hand, removal of the ASM-related signal results in a surface ozone increase of 34.4 ppbv from June to August, accounting for 81.5% of summertime ozone. This in turn results in the summertime surface ozone of Southern China exceeding that of Northern China by 11.5 ppbv and bears testimony to the crucial role played by the ASM in controlling lower ozone

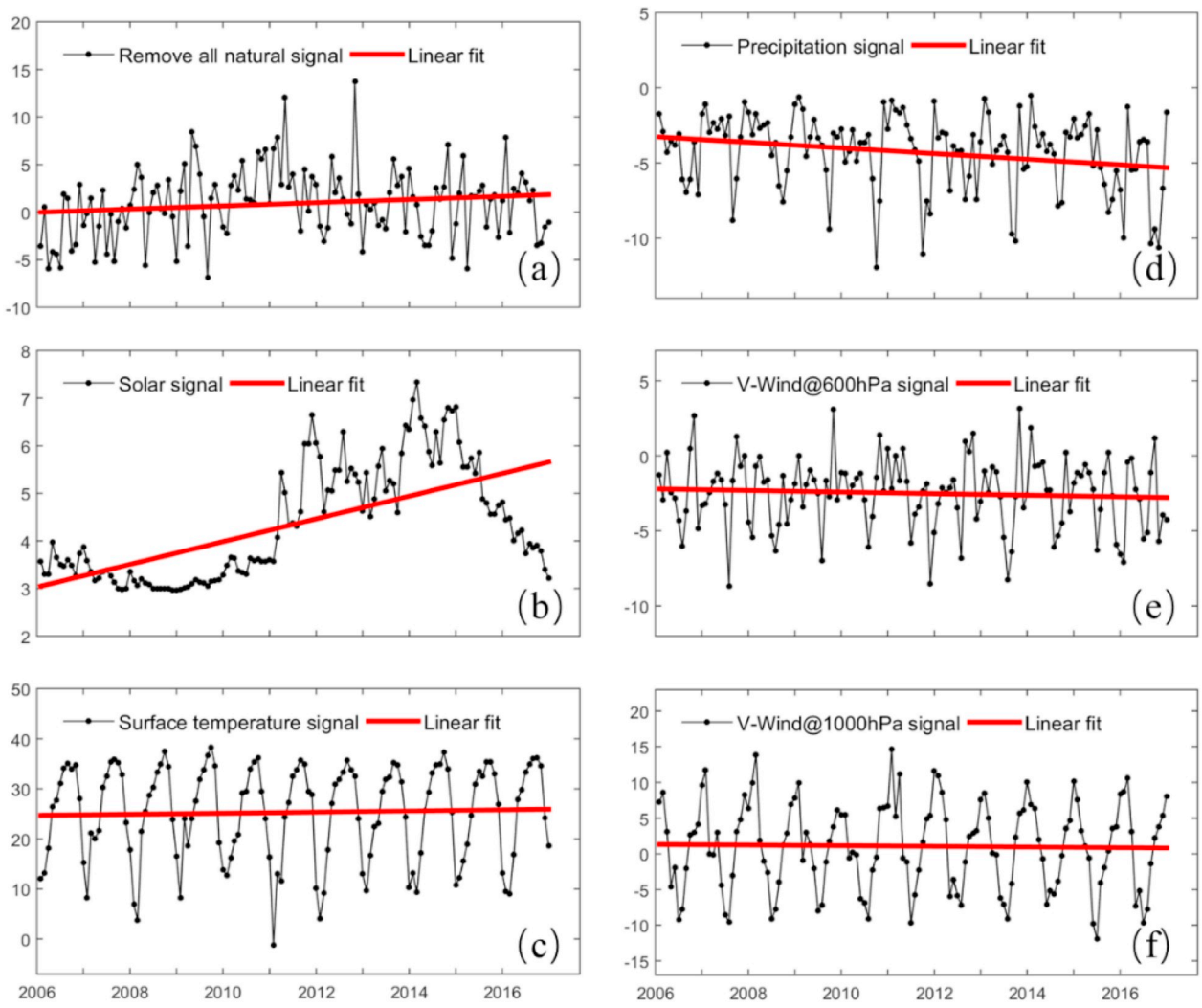

Fig. 7. Relative contributions of different signals to surface ozone variations over Southern China: (a) removed all natural signals, (b)solar cycle signal, (c) surface temperature signal, (d) precipitation signal, (e) V-wind@600 hPa signal, and (f) V-wind@1000 hPa signal.

Table 2
Comparison of trend analysis results between MK test and multiple linear regression.

Method		TCO (DU y^{-1})	Surface ozone (ppbv y^{-1})
Mann-kendall	Total	0.28	0.23
Linear fit based on MLR	Adjusted data after removing all natural signal	0.15*	0.17*
	Solar	0.10*	0.24*
	Precipitation	0.03	−0.19*
	Tropopause height	−0.01	\
	Surface temperature	\	0.11
	V–W ind@600 hPa	−0.01	−0.05
	V–W ind@1000 hPa	0.01	−0.05
	Total	0.27	0.23

Annual means interannual trend, "*" means the slope passes the significance test ($p < 0.05$). The "Total" at the bottom refers to the trends of modeled ozone from MLR.

levels in summertime over this region.

The role of the ASM-related signal in reducing summertime TCO and surface ozone over Southern China can be explained as follows: First, monsoons bring humid air from the marine sector, resulting in precipitation over land and associated wet scavenging of low-level ozone and its precursors (Zhao et al., 2010; Hou et al., 2015). At the same time, large cloud cover inhibits photochemical production of ozone (Bengal, 2014; Safieddine et al., 2015). Secondly, deep convective activity associated with rainfall transports ozone upwards, thereby reducing ozone in the entire tropospheric column (Dessler, 2002; Gettelman et al., 2002; Randel et al., 2010). Thirdly, horizontal transport of the ASM carries ozone-depleted marine air masses inland, resulting in dilution of tropospheric ozone (Zhao et al., 2010).

3.4. Discussion

Due to limitations related to non-continuous anthropogenic emission data for ozone precursors in this region, this study used only natural factors to develop the regression model. It is undeniable however that the impact of anthropogenic emissions on tropospheric ozone, especially surface ozone, could be significant. To demonstrate this, we removed variations in the ozone time series arising solely due to natural factors, and the results are shown in Figs. 6a and 7a. From the slope calculated in Table 2, it can be seen that there is still a 55.6% (0.15/0.27*100%) increase in TCO and 73.0% (0.17/0.23*100%) increase in surface ozone that remain unexplained. On the contrary, the natural factors can explain 44.4% (100 %–55.6%) and 27.0% (100 %–73.0%) of the respective increases. As shown in Fig. 6a, after the removal of natural factors, TCO exhibited a fluctuation between −7 and 16 DU, including a

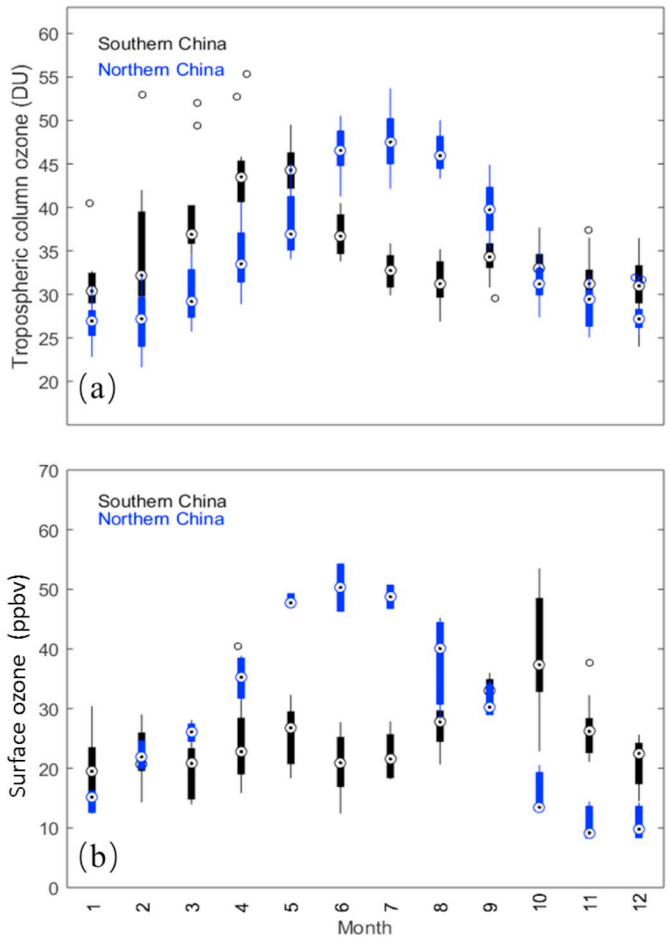

Fig. 8. Intra-annual cycle of TCO and surface ozone in Northern and Southern China: (a) tropospheric column ozone in Southern/Northern China (black/blue) and (b) surface ozone in Southern/Northern China (black/blue). The 'o' symbol denotes outliers. (For interpretation of the references to colour in this figure legend, the reader is referred to the Web version of this article.)

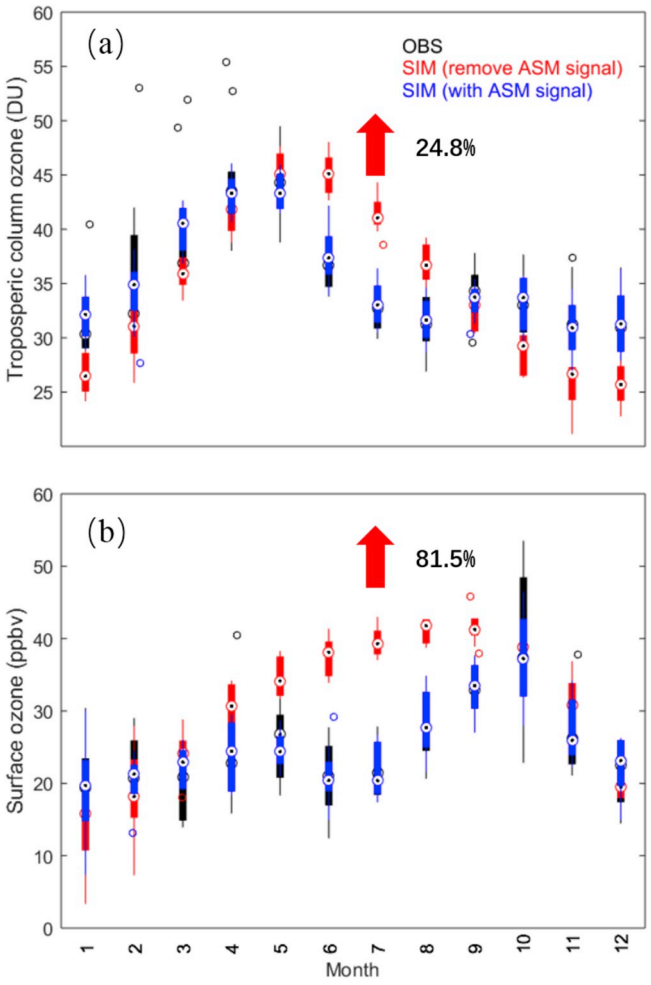

Fig. 9. Influence of the ASM-related signal on intra-annual variation of ozone: (a) tropospheric column ozone and (b) surface ozone. The 'o' symbol denotes outliers.

significant upward trend with a slope of 0.15 DU y^{-1} and unusually high values in 2011, 2012, and 2014, which could possibly reflect anthropogenic impacts or extreme meteorological conditions and changes in emissions from natural sources. However, surface ozone showed a fluctuation between −8 and 15 ppbv (Fig. 7a), including a significant upward trend of 0.16 ppbv y^{-1}. Although the overall trend is rising, the unexplained component changes with some increase until 2012–2013 and then some decrease. We conducted a seasonal analysis of unexplained ozone variations, and the results showed that the uptrend of ozone is mainly concentrated in spring and summer (Table S1). Studies have shown that anthropogenic NOx emissions in China are estimated to have decreased by 21% during 2013–2017, whereas volatile organic compound (VOC) emissions changed little (Li et al., 2018). Because the major cities in Southern China are in a VOC-sensitive region, the reduction in NOx will lead to an increase in ozone (Chen et al., 2019; Ou et al., 2016). In addition, the decline rate of NOx emissions in Southern China from June to September is greater than for other months (Gu et al., 2013), which is consistent with the highest uptrend of surface ozone in summer. In the future, numerical models can be used for further targeted analysis of the impacts of anthropogenic emissions on ozone levels in this region.

4. Conclusions

In this study, we used satellite- and ground-based measurements of TCO and surface ozone in Southern China to investigate the impacts of natural factors on long-term ozone trends. The main conclusions are as follows: First, a Mann-Kendall trend test analysis showed that within our research periods, both surface ozone and TCO over Southern China showed significant upward trends, with slopes of 0.97% y^{-1} (0.23 ppbv y^{-1}) and 0.82% y^{-1}r (0.28 DU y^{-1}), respectively. TCO exhibited an upward trend across all seasons, while surface ozone increased substantially only during summer. Secondly, among the large-scale atmospheric processes, the 11-year solar cycle had a crucial influence on both TCO and surface ozone, while ENSO, QBO, and AO did not play significant roles in constraining tropospheric ozone. Thirdly, among local-scale meteorological factors, precipitation, surface temperature, and zonal winds were observed to strongly significant effects on surface ozone, with middle- and low-level winds exhibiting a greater influence than high-level winds. Fourthly, the precipitation and wind fields associated with the ASM were critical in constraining lower ozone levels in summertime over Southern China, accounting for 24.8% and 81.5% of TCO and surface ozone variability, respectively. Finally, a significant fraction of TCO and surface ozone uptrends (55.6% and 73.0%, respectively) remain unexplained even after consideration of these natural factors. This discrepancy is most likely associated with anthropogenic emissions, which, based on our analysis, have a higher relative contribution to surface ozone than to TCO. This calls for future targeted studies to quantify the impacts from anthropogenic emissions on tropospheric ozone in Southern China.

Declaration of competing interest

The authors declare that they have no known competing financial interests or personal relationships that could have appeared to influence the work reported in this paper.

Acknowledgments

This work was supported by the National Nature Science Fund for Distinguished Young Scholars (41425020), the China Special Fund for Meteorological Research in the Public Interest (GYHY201206015), the National Key R&D Program of China (2017YFC0210105 and 2016YFC0202206) and Collaborative Innovation Center of Climate Change, Jiangsu province, China.

Appendix A. Supplementary data

Supplementary data to this article can be found online at https://doi.org/10.1016/j.atmosenv.2019.117060.

References

Abdul-Wahab, S.A., Bakheit, C.S., Al-Alawi, S.M., 2005. Principal component and multiple regression analysis in modelling of ground-level ozone and factors affecting its concentrations. Environ. Model. Softw 20, 1263–1271. https://doi.org/10.1016/j.envsoft.2004.09.001.

Baldwin, M., Gray, L., Dunkerton, T., Hamilton, K., Haynes, P., Randel, W., Holton, J., Alexander, M., Hirota, I., Horinouchi, T., Jones, D., Kinnersley, J., Marquardt, C., Sato, K., Takahashi, M., 2001. The quasi-biennial oscillation. Rev. Geophys. 39, 179–229.

Beig, G., Singh, V., 2007. Trends in tropical tropospheric column ozone from satellite data and MOZART model. Geophys. Res. Lett. 34, 1–5. https://doi.org/10.1029/2007GL030460.

Bengal, W., 2014. The role of tropospheric ozone and surface temperature on the forecasting of Indian summer monsoon. Rainfall Over Gangetic 2, 94–107.

Chandra, S., Ziemke, J.R., Stewart, R.W., 1999. An 11-year solar cycle in tropospheric ozone from TOMS measurements. Geophys. Res. Lett. 26 (2), 185–188.

Chandra, S., Ziemke, J.R., Martin, R.V., 2003. Tropospheric ozone at tropical and middle latitudes derived from TOMS/MLS residual: comparison with a global model. Journal of Geophysical Research-atmospheres 108 (D9).

Chang, K., Petropavlovskikh, I., Cooper, O.R., Schultz, M.G., 2017. Regional Trend Analysis of Surface Ozone Observations from Monitoring Networks in Eastern North America , Europe and East Asia 1–22.

Che, W., Zheng, J., Wang, S., Zhong, L., Lau, A., 2011. Assessment of motor vehicle emission control policies using Model-3/CMAQ model for the Pearl River Delta region, China. Atmos. Environ. Times 45, 1740–1751. https://doi.org/10.1016/j.atmosenv.2010.12.050.

Chehade, W., Weber, M., Burrows, J.P., 2014. Total ozone trends and variability during 1979-2012 from merged data sets of various satellites. Atmos. Chem. Phys. 14, 7059–7074. https://doi.org/10.5194/acp-14-7059-2014.

Chen, S., Goo, Y.J., Shen, Z., 2014. A hybrid approach of stepwise regression, logistic regression, support vector machine, and decision tree for forecasting fraudulent financial statements. Sci. World J. 1–9, 2014.

Chen, X., Situ, S., Zhang, Q., Wang, X., Sha, C., Zhouc, L., Wu, L., Wu, L., Ye, L., Li, C., 2019. The synergetic control of NO 2 and O 3 concentrations in a manufacturing city of southern China. Atmos. Environ. 201, 402–416. https://doi.org/10.1016/j.atmosenv.2018.12.021.

Chen, Z., Zhuang, Y., Xie, X., Chen, D., Cheng, N., Yang, L., Li, R., 2018. Understanding long-term variations of meteorological influences on ground ozone concentrations in Beijing during 2006–2016. Environ. Pollut. 245, 29–37.

Cooper, O.R., Parrish, D.D., Ziemke, J.R., 2014. Global distribution and trends of tropospheric ozone: an observation-based review. Elementa: Science of the Anthropocene 2, 1–28.

Deland, M.T., Cebula, R.P., 2008. Creation of a composite solar ultraviolet irradiance dataset. J. Geophys. Res. 113 (A11103).

Dessler, a.E., 2002. The effect of deep, tropical convection on the tropical tropopause layer. J. Geophys. Res. 107, 4033. https://doi.org/10.1029/2001JD000511.

Doherty, R.M., Stevenson, D.S., Johnson, C.E., Collins, W.J., Sanderson, M.G., 2006. Tropospheric ozone and El Niño–Southern Oscillation: influence of atmospheric dynamics, biomass burning emissions, and future climate change. J. Geophys. Res. 111, D19304. https://doi.org/10.1029/2005JD006849.

Edwards, R.P., Sale, O., Morris, G.A., 2018. Evaluation of El niño-southern oscillation in fluence on 30 years of tropospheric ozone concentrations in houston. Atmos. Environ. 192, 72–83. https://doi.org/10.1016/j.atmosenv.2018.08.032.

Fishman, J., Watson, C.E., Larsen, J.C., 1990. Distribution of tropospheric ozone determined from satellite data. J. Geophys. Res. 95, 3599–3617.

Fishman, J., Wozniak, A.E., Creilson, J.K., 2003. Global distribution of tropospheric ozone from satellite measurements using the empirically corrected tropospheric ozone residual technique: identification of the regional aspects of air pollution. Atmos. Chem. Phys. 3, 893–907.

Fishman, J., Creilson, J.K., Wozniak, A.E., 2005. Interannual variability of stratospheric and tropospheric ozone determined from satellite measurements. J. Geophys. Res. 110 (D20306).

Fleming, Z.L., Doherty, R.M., Von Schneidemesser, E., Malley, C.S., Cooper, O.R., Pinto, J.P., Colette, A., Xu, X., Simpson, D., Schultz, M.G., Lefohn, A.S., Hamad, S., Moolla, R., Solberg, S., 2018. Tropospheric Ozone Assessment Report : Present-Day Ozone Distribution and Trends Relevant to Human Health.

Fusco, A.C., Salby, M.L., 1999. Interannual variations of total ozone and their relationship to variations of planetary wave activity. J. Clim. 12, 1619–1629. https://doi.org/10.1175/1520-0442(1999)012<1619:IVOTOA>2.0.CO, 2.

Gettelman, A., Salby, M.L., Sassi, F., 2002. Distribution and influence of convection in the tropical tropopause region. J. Geophys. Res. Atmos. 107 https://doi.org/10.1029/2001JD001048.

Gocic, M., Trajkovic, S., 2013. Analysis of changes in meteorological variables using Mann-Kendall and Sen's slope estimator statistical tests in Serbia. Glob. Planet. Chang. 100, 172–182. https://doi.org/10.1016/j.gloplacha.2012.10.014.

Greenslade, J.W., Alexander, S.P., Schofield, R., Fisher, J.A., Klekociuk, A.K., 2017. Stratospheric ozone intrusion events and their impacts on tropospheric ozone in the Southern Hemisphere. Atmos. Chem. Phys. 17, 10269–10290. https://doi.org/10.5194/acp-17-10269-2017.

Gu, D., Wang, Y., Smeltzer, C., Liu, Z., 2013. Reduction in NOx emission trends over China: regional and seasonal variations. Environ. Sci. Technol. 47, 12912–12919. https://doi.org/10.1021/es401727e.

Guangdong Provincial Environmental Monitoring Centre and Environmental Protection Department, 2006. Guangdong-Hong Kong-Macao Pearl River Delta Regional Air Quality Monitoring Network.

Guangdong Provincial Environmental Monitoring Centre and Environmental Protection Department, 2014. Guangdong-Hong Kong-Macao Pearl River Delta Regional Air Quality Monitoring Network.

Haman, C.L., Couzo, E., Flynn, J.H., Vizuete, W., Heffron, B., Lefer, B.L., 2014. Relationship between boundary layer heights and growth rates with ground-level Ozone in Houston, Texas. J. Geophys. Res. 119, 6230–6245. https://doi.org/10.1002/2013JD020473.

Holton, J.R., Haynes, P.H., Mcintyre, M.E., Douglass, A.R., Rood, B., 1995. STRATOSPHERE-TROPOSPHERE 403–439.

Hou, X., Zhu, B., Fei, D., Wang, D., 2015. The impacts of summer monsoons on the ozone budget of the atmospheric boundary layer of the Asia-Pacific region. Sci. Total Environ. 502, 641–649. https://doi.org/10.1016/j.scitotenv.2014.09.075.

Huang, F.-X., Liu, N.-Q., Zhao, M.-X., 2009. Solar cycle signal of tropospheric ozone over the Tibetan Plateau. Acta Geophys. Sin. 52 https://doi.org/10.3969/j.issn.0001-5733.2009.09.003.

Huang, F.X., Jiang, Y., Huang, G.D., Zhang, X.X., 2013. Construction of long-time series of solar extreme ultraviolet radiation with F10.7 and Mg II. Chin. J. Geophys. 56 (9), 2912–2917.

IPCC (Intergovernmental Panel on Climate Change), 2013. Working group I contribution to the IPCC fifth assessment Report "climate change 2013: the physical science basis", final draft underlying scientific-technical assessment. Available at: http://www.ipcc.ch.

Jiang, F., Wang, T., Wang, T., Xie, M., Zhao, H., 2008. Numerical modeling of a continuous photochemical pollution episode in Hong Kong using. WRF – chem 42, 8717–8727. https://doi.org/10.1016/j.atmosenv.2008.08.034.

Kulkarni, P.S., Ghude, S.D., Bortoli, D., 2010. Tropospheric ozone trend over three major inland indian cities: Delhi, Hyderabad and Bangalore. Ann. Geophys. 28, 1879–1885.

Lal, D.M., Ghude, S.D., Patil, S.D., Kulkarni, S.H., Jena, C., Tiwari, S., Srivastava, M.K., 2012. Tropospheric ozone and aerosol long-term trends over the Indo-Gangetic Plain (IGP), India. Atmos. Res. 116, 82–92. https://doi.org/10.1016/j.atmosres.2012.02.014.

Lee, Y.C., Shindell, D.T., Faluvegi, G., Wenig, M., Lam, Y.F., Ning, Z., Hao, S., Lai, C.S., 2014. Increase of ozone concentrations, its temperature sensitivity and the precursor factor in South China. Tellus Ser. B Chem. Phys. Meteorol. 66, 1–16. https://doi.org/10.3402/tellusb.v66.23455.

Li, K., Jacob, D.J., Liao, H., Shen, L., Zhang, Q., Bates, K.H., 2018. Anthropogenic drivers of 2013 – 2017 trends in summer surface ozone in China 1–6. .

Li, S., Wang, T., Huang, X., Pu, X., Li, M., Chen, P., Yang, X.Q., Wang, M., 2018. Impact of east asian summer monsoon on surface ozone pattern in China. J. Geophys. Res. Atmos. 123, 1401–1411. https://doi.org/10.1002/2017JD027190.

Lin, M., Horowitz, L.W., Oltmans, S.J., 2014. Tropospheric ozone trends at Mauna Loa observatory tied to decadal climate variability. Nat. Geosci. 7, 136–143.

Logan, J.A., 1985. Tropospheric ozone: seasonal behavior, trends, and anthropogenic influence. J. Geophys. Res. Atmos. 90, 10463–10482.

Lou, S., et al., 2015. Simulation of the interannual variations of tropospheric ozone over China: roles of variations in meteorological parameters and anthropogenic emissions. Atmos. Environ. 122, 839–851.

McAdams, H.T., Crawford, R.W., Hadder, G.R., 2000. A Vector Approach to Regression Analysis and its Application to Heavy-Duty Diesel Emissions. Society of Automotive Engineers, Inc, Contract with the Energy Division of Oak Ridge National Laboratory (ORNL). Contract No. DE-AC05-00OR22725.

Mills, G., Pleijel, H., Malley, C.S., Sinha, B., Cooper, O.R., Schultz, M.G., Neufeld, H.S., Simpson, D., Sharps, K., Gerosa, G., Harmens, H., Kobayashi, K., Saxena, P., 2018. Tropospheric Ozone Assessment Report : Present-Day Tropospheric Ozone Distribution and Trends Relevant to Vegetation.

Mohnen, V.A., Goldstein, W., Wang, W.C., 1993. Tropospheric ozone and climate change. Air Waste 43, 1332–1334.

Muralidharan, V., Kumar, G.M., Sampath, S., 1989. Surface ozone variation associated with rainfall. Pure Appl. Geophys. PAGEOPH 130, 47–55. https://doi.org/10.1007/BF00877736.

Nassar, R., Logan, J.A., Megretskaia, I.A., 2009. Analysis of tropical tropospheric ozone, carbon monoxide, and water vapor during the 2006 El Nino using TES observations and the GEOS-Chem model. J. Geophys. Res. 114 (D17304).

Oltmans, S.J., Lefohn, A.S., Harris, J.M., Galbally, I., Scheel, H.E., Bodeker, G., Brunke, E., Claude, H., Tarasick, D., Johnson, B.J., Simmonds, P., Shadwick, D., Anlauf, K., Hayden, K., Schmidlin, F., Fujimoto, T., Akagi, K., Meyer, C., Nichol, S., Davies, J., Redondas, A., Cuevas, E., 2006. Long-term changes in tropospheric ozone. Atmos. Environ. 40, 3156–3173. https://doi.org/10.1016/j.atmosenv.2006.01.029.

Oltmans, S.J., Lefohn, A.S., Shadwick, D., Harris, J.M., Scheel, H.E., Galbally, I., Tarasick, D.W., Johnson, B.J., Brunke, E.G., Claude, H., Zeng, G., Nichol, S., Schmidlin, F., Davies, J., Cuevas, E., Redondas, A., Naoe, H., Nakano, T., Kawasato, T., 2013. Recent tropospheric ozone changes - a pattern dominated by slow or no growth. Atmos. Environ. 67, 331–351. https://doi.org/10.1016/j.atmosenv.2012.10.057.

Oman, L.D., Ziemke, J.R., Douglass, A.R., Waugh, D.W., Lang, C., Rodriguez, J.M., Nielsen, J.E., 2011. The response of tropical tropospheric ozone to ENSO. Geophys. Res. Lett. 38, 2–7. https://doi.org/10.1029/2011GL047865.

Ou, J., Yuan, Z., Zheng, J., Huang, Z., Shao, M., Li, Z., Huang, X., Guo, H., Louie, P.K.K., 2016. Ambient ozone control in a photochemically active region: short- term despiking or long-term attainment? Environ. Sci. Technol. 50, 5720–5728. https://doi.org/10.1021/acs.est.6b00345.

Randel, W.J., Cobb, J.B., 1994. Coherent variations of monthly mean total ozone and lower stratospheric temperature. J. Geophys. Res. 99, 5433–5447.

Randel, W.J., Park, M., Emmons, L., Kinnison, D., Bernath, P., Walker, K.A., Boone, C., Pumphrey, H., 2010. Asian monsoon transport of pollution to the stratosphere. Science 80 (328), 611–613. https://doi.org/10.1126/science.1182274.

Safieddine, S., Boynard, A., Hao, N., Huang, F., Wang, L., Ji, D., Barret, B., Ghude, S.D., Coheur, P.F., Hurtmans, D., Clerbaux, C., 2015. Tropospheric ozone variability during the east asian summer monsoon as observed by satellite (IASI), aircraft (MOZAIC) and ground stations. Atmos. Chem. Phys. Discuss. 15, 31925–31950. https://doi.org/10.5194/acpd-15-31925-2015.

Shen, L., Wang, Y., 2012. Changes in tropospheric ozone levels over the three representative regions of China observed from space by the tropospheric emission spectrometer (TES), 2005-2010. Chin. Sci. Bull. 57, 2865–2871. https://doi.org/10.1007/s11434-012-5099-x.

Steinbrecht, W., Köhler, U., Claude, H., Weber, M., Burrows, J.P., Van Der A, R.J., 2011. Very high ozone columns at northern mid-latitudes in 2010. Geophys. Res. Lett. 38, 1–5. https://doi.org/10.1029/2010GL046634.

Sun, L., et al., 2019. Impacts of meteorology and emissions on summertime surface ozone increases over central eastern China between 2003 and 2015. Atmos. Chem. Phys. 19, 1455–1469.

Tang, G., Li, X., Wang, Y., Xin, J., Ren, X., 2009. Surface ozone trend details and interpretations in Beijing, 2001–2006. Atmos. Chem. Phys. 8813–8823, 9. www.atmos-chem-phys.net/9/8813/2009/.

Uno, I., Carmichael, R., Phadnis, J., Zha, Y., Sunwoo, Y., 1998. Tropospheric ozone production and transport in the springtime in east Asia. J. Geophys. Res. 103, 10649–10671. https://doi.org/10.1029/97JD03740.

Wang, S., Hao, J., 2012. Air quality management in China: issues, challenges, and options. J. Environ. Sci. 24, 2–13. https://doi.org/10.1016/S1001-0742(11)60724-9.

Wang, T., Wei, X.L., Ding, A.J., Poon, C.N., Lam, K.S., Li, Y.S., Chan, L.Y., Anson, M., 2009. Increasing surface ozone concentrations in the background atmosphere of Southern China, 1994-2007. Atmos. Chem. Phys. 9, 6217–6227. https://doi.org/10.5194/acp-9-6217-2009.

Wang, Z., Pochanart, P., Li, J., Akimoto, H., 2008. Significant impact of the East Asia monsoon on ozone seasonal behavior in the boundary layer of Eastern China and the west Pacific region. .

Worden, J., Jones, D.B.A., Liu, J., Parrington, M., Bowman, K., Stajner, I., Beer, R., Jiang, J., Thouret, V., Kulawik, S., Li, J.L.F., Verma, S., Worden, H., 2009. Observed vertical distribution of tropospheric ozone during the Asian summertime monsoon. J. Geophys. Res. Atmos. 114 https://doi.org/10.1029/2008JD010560.

Wu, X.K., Qie, X.S., Yuan, T., 2013. Regional distribution and diurnal variation of deep convective systems over the Asian monsoon region. Sci. China Earth Sci. 56, 843–854. https://doi.org/10.1007/s11430-012-4551-8.

Xu, W., Xu, X., Lin, M., Lin, W., Tarasick, D., Tang, J., Ma, J., Zheng, X., 2018. Long-term trends of surface ozone and its influencing factors at the Mt Waliguan GAW station, China - Part 2: the roles of anthropogenic emissions and climate variability. Atmos. Chem. Phys. 18, 773–798. https://doi.org/10.5194/acp-18-773-2018.

Young, P.J., Naik, V., Fiore, A.M., Gaudel, A., Guo, J., Lin, M.Y., Neu, J.L., 2018. Tropospheric Ozone Assessment Report : Assessment of Global-Scale Model Performance for Global and Regional Ozone Distributions , Variability , and Trends.

Zhang, Y., Zhao, L., Wang, W., Tang, S., 2018. FY3/TOU satellite data and impacts of East Asian summer monsoon. .

Zhao, C., Wang, Y., Yang, Q., Fu, R., Cunnold, D., Choi, Y., 2010. Impact of East Asian summer monsoon on the air quality over China: view from space. J. Geophys. Res. Atmos. 115, 1–12. https://doi.org/10.1029/2009JD012745.

Zhao, E.R., Jian, M.Q., Li, C.H., 2018. Interdecadal change of the seasonal evolution of rainfall over South China. J. Trop. Meteorol. 34 (3), 360–370.

Zhong, L., Louie, P.K.K., Zheng, J., Yuan, Z., Yue, D., Ho, J.W.K., Lau, A.K.H., 2013. Science-policy interplay: air quality management in the Pearl River Delta region and Hong Kong. Atmos. Environ. 76, 3–10. https://doi.org/10.1016/j.atmosenv.2013.03.012.

Zhou, H., Zhou, C., Lynam, M.M., Dvonch, J.T., Barres, J.A., Hopke, P.K., Cohen, M., Holsen, T.M., 2017. Atmospheric mercury temporal trends in the northeastern United States from 1992 to 2014: are measured concentrations responding to decreasing regional emissions? Environ. Sci. Technol. Lett. 4, 91–97. https://doi.org/10.1021/acs.estlett.6b00452.

Ziemke, J.R., Chandra, S., Bhartia, P.K., 1998. Two new methods for deriving tropospheric column ozone from TOMS measurements: assimilated UARS MLS/HALOE and convective-cloud differential techniques. J. Geophys. Res. 103, 22115–22127.

Ziemke, J.R., Chandra, S., 1999. Seasonal and interannual variabilities in tropical tropospheric ozone. J. Geophys. Res. 104 (D17), 21425–21442.

Ziemke, J.R., Chandra, S., Bhartia, P.K., 2000. A new NASA data product: tropospheric and stratospheric column ozone in the tropics derived from TOMS measurements. Bull. Am. Meteorol. Soc. 81 (3), 580–583.

Ziemke, J.R., Chandra, S., Bhartia, P.K., 2005. A 25-year data record of atmospheric ozone in the Pacific from Total Ozone Mapping Spectrometer (TOMS) cloud slicing: implications for ozone trends in the stratosphere and troposphere. J. Geophys. Res. D Atmos. 110, 1–15. https://doi.org/10.1029/2004JD005687.

Ziemke, J.R., Chandra, S., Duncan, B.N., 2006. Tropospheric ozone determined from Aura OMI and MLS: evaluation of measurements and comparison with the global modeling initiative's chemical transport model. J. Geophys. Res. 111 (D19303).

Ziemke, J.R., Chandra, S., Oman, L.E., 2010. A new ENSO index derived from satellite measurements of column ozone. Atmos. Chem. Phys. 10, 3711–3721.

Ziemke, J.R., Chandra, S., Labow, G.J., 2011. A global climatology of tropospheric and stratospheric ozone derived from Aura OMI and MLS measurements. Atmos. Chem. Phys. 11, 9237–9251.

Ziemke, J.R., Oman, L.D., Strode, S.A., Douglass, A.R., Olsen, M.A., Mcpeters, R.D., Bhartia, P.K., Froidevaux, L., Labow, G.J., Witte, J.C., Thompson, A.M., Haffner, D. P., Kramarova, N.A., Frith, S.M., Huang, L., Jaross, G.R., Seftor, C.J., Deland, M.T., Taylor, S.L., Ziemke, C.J.R., 2019. Trends in Global Tropospheric Ozone Inferred from a Composite Record of TOMS/OMI/MLS/OMPS Satellite Measurements and the MERRA-2 GMI Simulation, pp. 3257–3269.